

Experimental communication

Cite

Cecatto C, Cardoso LHD, Ozola M, Korzh S, Zvejniece L, Gukalova B, Doerrier C, Dambrova M, Gnaiger E, Makrecka-Kuka M, Liepinsh E (2023) Fatty acid β -oxidation in brain mitochondria: Insights from high-resolution respirometry in mouse, rat and *Drosophila* brain, ischemia and aging models. MitoFit Preprints 2023.10. <https://doi.org/10.26124/mitofit:2023-0010>

Author contributions

Conceptualization: CC, LHDC, MO, MD, CD, EG, MMK, EL; methodology: CC, LHDC, MO, BG, EG, MMK; formal analysis: CC, LHDC; visualization: CC, LHDC; investigation (experiments performance): MO, SK, LZ, BG, CD, MMK; writing-original draft: CC, LHDC, MO, MD, MMK, EL; writing-review and editing: CC, LHDC, MO, SK, LZ, BG, CD, MD, EG, MMK, EL.

Conflicts of interest

EG is founder and CEO of Oroboros Instruments, Innsbruck, Austria; the other authors declare no conflict of interest.

Online 2023-11-22












Data availability

The data that support the findings of this study are available from the authors upon reasonable request.

Keywords

brain;
nervous system;
mitochondrial function;
fatty acid oxidation;
beta-oxidation;
acylcarnitines;
respirometry.

Fatty acid β -oxidation in brain mitochondria: Insights from high-resolution respirometry in mouse, rat and *Drosophila* brain, ischemia and aging models

 Cristiane Cecatto^{1*},  Luiza H. D. Cardoso^{1*#},  Melita Ozola^{2,3},  Stanislava Korzh²,  Liga Zvejniece²,  Baiba Gukalova^{2,3},  Carolina Doerrier¹,  Maija Dambrova^{2,3},  Erich Gnaiger¹,  Marina Makrecka-Kuka²,  Edgars Liepinsh^{2,3}

1 Oroboros Instruments, Innsbruck, Austria;

2 Latvian Institute of Organic Synthesis Laboratory of Pharmaceutical Pharmacology, Riga, Latvia;

3 Faculty of Pharmacy, Riga Stradins University, Riga, Latvia

* These authors contributed equally to this work.

Corresponding author: luiza.cardoso@oroboros.at

Summary

Glucose is the main energy source of the brain, yet recent studies demonstrate that fatty acid oxidation (FAO) plays a relevant role in the pathogenesis of central nervous system disorders. We evaluated FAO in brain mitochondria under physiological conditions, in the aging brain, and after stroke.

Using high-resolution respirometry we compared medium-chain (MC, octanoylcarnitine) and long-chain (LC, palmitoylcarnitine) acylcarnitines as substrates of β -oxidation in the brain. The capacity of FA oxidative phosphorylation (F-OXPHOS) with palmitoylcarnitine was up to 4 times higher than respiration with octanoylcarnitine. The optimal concentration of palmitoylcarnitine was 10 μ M which corresponds to the total concentration of LC acylcarnitines in the brain. Maximal respiration with octanoylcarnitine was reached at 20 μ M, however, this concentration exceeds MC acylcarnitine concentrations in the brain 15 times. The protocols

developed avoid FAO overestimation by malate-linked anaplerotic activity in brain mitochondria. F-OXPPOS capacity was highest in mouse cerebellum, intermediate in cortex, prefrontal cortex, and hypothalamus, and hardly detectable in hippocampus. F-OXPPOS capacity was 2-fold lower and concentrations of LC acylcarnitines were 2-fold higher in brain of aged rats. A similar trend was observed in the rat model of endothelin-1-induced stroke. In conclusion, although FAO is not a dominant pathway in brain bioenergetics, it deserves specific attention in studies of brain metabolism.

1. Introduction

Brain function depends on aerobic mitochondrial energy metabolism of glucose, lactate, and ketones, but the role of fatty acid oxidation (FAO) is controversial. Fatty acids are both transported and metabolized in the brain ^{1,2}. The pattern of core energy metabolism differs among cell types: FAO occurs in astrocytes but not in neurons ^{3,4}. A high-fat diet increased the levels of lipids and reduced cytochromes in astrocytes but not in neurons of mice ⁵.

Acyl-CoA are formed in the cytosol, which are then available for further metabolic reactions, including the formation of acylcarnitines by exchange of CoA with carnitine by carnitine palmitoyltransferase 1 (CPT1). A liver-type CPT1A isoform is found in astrocytes ³. Acylcarnitines can be transported to other cells or enter mitochondria through carnitine acylcarnitine translocase (CAT) located in the mitochondrial inner membrane (mtIM) ⁶. In the mitochondrial matrix, acylcarnitine is converted into acyl-CoA by CPT2. In healthy mitochondria, acyl-CoA is immediately broken down into acetyl-CoA in the β -oxidation cycle, further oxidized in the TCA cycle, and finally in the membrane-bound electron transfer system (membrane-ETS).

β -oxidation is initiated in the mitochondrial matrix by acyl-CoA dehydrogenases (ACADs), which dehydrogenate acyl-CoA, reducing the enzyme's FAD prosthetic group to FADH₂. Further H⁺-linked electron transfer is mediated by electron-transferring flavoprotein (ETF)⁷ reducing FAD in the electron-transfer flavoprotein ubiquinone oxidoreductase (ETF-QO or ETFDH) ^{8,9}. ETFDH is effectively an integral membrane-ETS Complex (CETFDH) that catalyzes the reduction of coenzyme Q ¹⁰⁻¹³

Many pathways converge at the Q-junction, to reduce the electron transfer system-reactive CoQ (Q) ¹⁴. Q is oxidized by Complex III (CIII), after which the electrons are transferred to cytochrome *c* and sequentially to Complex IV, which reduces O₂ to H₂O. This allows measurement of FAO by respirometry ¹⁵.

β -oxidation generates NADH from the 3-hydroxyacyl-CoA dehydrogenase reaction in the mitochondrial trifunctional protein (TFP or MTP), which receives the products from various ACADs ¹⁶. NADH is oxidized by Complex I (CI), which reduces Q. In this way, FAO depends on two different entries of electrons into the membrane-ETS through ETF into CETFDH and NADH into CI. ¹¹

Acetyl-CoA is produced during each β -oxidation cycle when the FA chains are shortened by 2 carbons. Acetyl-CoA enters the TCA cycle through condensation with

oxaloacetate by citrate synthase. To avoid acetyl-CoA accumulation, which would block FAO, the addition of malate is necessary in respirometry with mitochondrial preparations, to provide oxaloacetate by malate dehydrogenase^{12,17}. However, it is little discussed in the literature that the presence of mitochondrial malic enzyme might pose a problem when using malate for FAO analysis: this enzyme, involved in anaplerosis, converts malate into pyruvate, thus enabling the TCA cycle enzymes to produce NADH independent of FAO. This leads to overestimation of FAO. Therefore, careful assessment of protocols is required to quantify FAO accurately by respirometry¹⁸.

With high-resolution respirometry (HRR), it is possible to measure FAO in mitochondrial preparations such as isolated mitochondria, tissue homogenate, permeabilized cells, and permeabilized fibers. Different FA of varying length or conjugated to CoA or carnitine can be used to measure FAO capacities. FAs can be divided by chain length into short-chain (SC, 2–5 carbons), medium-chain (MC, 6–12 carbons), long-chain (LC, 13–20) and very long-chain (VLC, >21 carbons) FA. While SC and MCFA can enter the mitochondrial matrix, LCFA must be bound to carnitine by carnitine acyltransferase to enter the mitochondrial matrix¹⁹. Thus, acylcarnitines are frequently employed to study mitochondrial FAO. Combinations of acyl-CoA and carnitine are used less frequently, as the reaction of carnitine acyltransferase (carnitine palmitoyltransferase, CPT-1) is considered a regulatory node controlling FAO rates²⁰.

It is widely hypothesized that neurons receive metabolic support from astrocytes by delivering metabolites such as ketones, acetyl-CoA, and acylcarnitines that are taken up and utilized by neurons²¹. Thus, metabolic processes in neurons depend on FAO in astrocytes that generate a variety of metabolites. While several methods have been developed to assess metabolism in the brain *in vivo*²², *ex vivo* analyses are complementary to investigate metabolism and test interventions.

Several studies have shown that plasma/serum levels of acylcarnitines, especially MC and LC acylcarnitines, are elevated in patients with diabetes mellitus, cancer, heart failure, and septic shock^{6,23}. The content of LC acylcarnitines in adult and aged male mice is elevated after stroke, and LC acylcarnitines accumulate in the brain with aging²⁴. However, the physiological and pathological roles of MC and LC acylcarnitines in brain tissue mitochondrial function are unknown.

In the present study, we evaluated the effect of MC and LC acylcarnitines on FAO and their contribution to mitochondrial brain respiration. We compared different mouse tissues, brain regions, and brain from different species. Finally, we determined the effect of ischemia and aging on FAO in brain.

2. Materials and Methods

2.1. Chemicals

Endothelin-1 (ET-1), isoflurane, oxygen and nitrous oxide gases, tramadol, and sterile 0.9 % NaCl solution (saline) were purchased from Tocris Bioscience (Bristol, United Kingdom), ABOTT (Maidenhead, Great Britain), AGA (Riga, Latvia), KRKA (Novo mesto, Slovenia) and Fresenius Kabi (Warszawa, Poland), respectively. All other reagents were purchased from Sigma-Aldrich (Schnelldorf, Germany).

2.2. Animals

All animal care and experimental procedures complied with the guidelines reported in EU Directive 2010/63/EU and with local laws and policies and were approved by the Ethics Council of Animal Protection at the Veterinary and Food Service, Riga, Latvia (ethical approvals No. 82 and 83) or were conducted following the Austrian Animal Experimentation Act (Tierversuchsgesetz 2012; Directive 2010/63/EU; BMWFM-66.011/0128-WF/V/3b/2016).

Male Sprague–Dawley outbred rats or male inbred Wistar rats were purchased from Envigo, Netherlands. C57bl/6N inbred mice were purchased from the Laboratory Animal Centre, University of Tartu (Estonia). The mice and rats were housed in separate rooms in individually ventilated cages (three rats per cage or five mice per cage), under standard conditions (21–23 °C, 65 % ± 10 % relative humidity, 12 h light–dark cycle) with unlimited access to standard food (R70 diet, Lactamin AB, Stockholm, Sweden) and water.

C57bl/6N wild-type young adult mice (male and female) were also obtained from the animal facility of the Medical University of Innsbruck and were housed in clear plastic cages (maximum five mice per cage) at 23 ± 3 °C under a 12/12 h light/dark cycle with access to food and water *ad libitum*.

C57Bl/6N 3 months old mice were used to compare MC and LC acylcarnitines as FA substrates and the FAO-dependent O₂ flux in different tissues and various brain regions.

CSORC strain *Drosophila melanogaster* wild-type flies, originated from crossing of CantonS and OregonR-C flies (Bloomington *Drosophila* Stock Center, Bloomington, IN, United States), were kept at 25 °C in an incubator with 60 % humidity on a 12/12-hour light/dark cycle. The flies were fed with Jazz-Mix *Drosophila* food with the addition of 8.3 % yeast extract (both from Fisher Scientific, Waltham, MA, USA).

Animal model of aging: To compare the brain energy metabolism of adult and aged rats, a natural aging model was chosen. For this experiment, we set two experimental groups ($N=6$ each): adult (8 months) and aged (20 months) Wistar rats. As the groups were supposed to differ significantly in age, Wistar rats were ordered from the same vendor with a time gap of 12 months and were housed under standard conditions. After reaching the specified age, the animals were sacrificed, and brain tissues were collected to analyze FAO and the acylcarnitine profile in brain homogenates.

Animal models for transient middle cerebral artery occlusion (MCAO): The Sprague–Dawley 8–10 week old rats were divided into experimental groups with $N=4$ each: sham-operated, and ET-1-induced MCAO rats with brain tissue collected 2 or 24 hours after.

The vasoconstrictive peptide ET-1 was used to induce MCAO²⁵. Briefly, the rats were anesthetized with 5 % isoflurane in a mixture of nitrous oxide and oxygen (30:70), and anesthesia was maintained with 2 % isoflurane using a face mask. The depth of anesthesia was monitored by toe pinch. After that, the rats received a subcutaneous injection of tramadol (10 mg·kg⁻¹) and were placed in a stereotaxic device (Stoelting Europe, Dublin, Ireland). A midline incision was made in the skin above the bregma, the skull was cleaned of surrounding tissue, and a small hole was drilled in the skull using a micromotor High-Speed Drill (Stoelting Europe, Dublin, Ireland). The stereotaxic coordinates for ET-1 microinjection were (relative to the bregma): 0.2 mm anterior, 5.1 mm lateral, and 8.2 mm ventral. These coordinates are adjacent to the middle cerebral artery (MCA) in the piriform cortex as described previously²⁶. ET-1 solution at a dose of 50 μmol·L⁻¹ was

injected at $1 \mu\text{L}\cdot\text{min}^{-1}$ using a $10 \mu\text{L}$ Hamilton syringe with a 26 s-gauge needle for 3.2 minutes, resulting in 160 pmol of ET-1 injected. Prior to slow withdrawal, the needle was left in the injection site for 3.5 min to prevent backflow of ET-1. The sham-operated animals were subjected to the same surgical procedure, and saline was used for microinjection.

After MCAO induction, brain tissue was collected for further analyses to detect mitochondrial function in risk and non-risk areas as well as acylcarnitine levels in the brain.

2.3. Determination of the acylcarnitine profile in brain tissue

The carnitine concentration and acylcarnitine profile in the brain homogenates were determined with ultra-performance liquid chromatography-tandem mass spectrometry (UPLC/MS/MS) 2 and 24 hours after ET-1-induced MCAO or at the endpoint of the aging experiment^{27,28}. The concentration of measured compounds was expressed as $\text{nmol}\cdot\text{mg}^{-1}$ of wet tissue mass.

2.4. Sample preparation for respirometric analyses

Mouse and rat tissues were collected in ice-cold BIOPS (10 mM Ca^{2+} -EGTA - $0.1 \mu\text{M}$ free Ca^{2+} , 20 mM imidazole, 20 mM taurine, 50 mM K^{+} -MES, 0.5 mM dithiothreitol, 6.56 mM MgCl_2 , 5.77 mM ATP , 15 mM phosphocreatine, pH 7.1 adjusted with KOH)²⁹. Brain and kidney tissue homogenates were prepared using a Teflon-glass pestle with mechanical homogenizer at 200 rpm, 10 strokes, at a wet mass concentration of $80 \text{ mg}\cdot\text{mL}^{-1}$ with mitochondrial respiration medium MiR05 (0.5 mM EGTA , 3 mM MgCl_2 , 60 mM lactobionic acid, 20 mM taurine, $10 \text{ mM KH}_2\text{PO}_4$, 20 mM HEPES , 110 mM sucrose, $1 \text{ g}\cdot\text{L}^{-1}$ BSA essentially free of FAs; pH 7.1)³⁰. Homogenate ($25 \mu\text{L}$) was added to the respirometric chambers to obtain a final concentration of $1 \text{ mg}\cdot\text{mL}^{-1}$. When indicated, protein was determined following the Lowry method³¹ and used for normalization of the data.

Cardiac fibers were permeabilized with saponin ($50 \mu\text{g}\cdot\text{mL}^{-1}$) in a modified BIOPS buffer (20 mM imidazole, 0.5 mM dithiothreitol, 20 mM taurine, 7.1 mM MgCl_2 , 50 mM MES , 5 mM ATP , 15 mM phosphocreatine, $2.6 \text{ mM CaK}_2\text{EGTA}$, $7.4 \text{ mM K}_2\text{EGTA}$; pH 7.0) for 15 minutes³². Between ~ 1.5 – 2 mg of fibers (wet mass) was transferred to the respirometric chambers.

Drosophila brains were dissected according to a previously published protocol³³. The same modified BIOPS buffer described above was chosen for brain dissection to preserve mitochondrial function until respirometric analysis, 10–12 brains were used per respirometric chamber and the data was normalized per wet mass.

2.5. High-resolution respirometry

Mitochondrial respiration was measured at $37 \text{ }^\circ\text{C}$ (mouse, rat) or $25 \text{ }^\circ\text{C}$ (*Drosophila*) using O2k high-resolution respirometers (Oroboros Instruments, Innsbruck, Austria) with 2 mL chambers with MiR05 supplemented with 20 mM creatine³⁴. Several substrate-uncoupler-inhibitor titration (SUIT) protocols were used: https://wiki.oroboros.at/index.php/FAT4BRAIN_FAO-mito-CNS_platform (retrieved on 2023-11-20).

For experiments with brain homogenate with different acylcarnitines and malate kinetics, the protocols SUIT-036, 037 and 038 with Pal, Oct and carrier, respectively, were used: after sample addition to the chambers, ADP was added at 5 mM, to stimulate oxidation of residual endogenous substrates (REN state). Afterwards, malate 0.1 mM was added, followed by palmitoylcarnitine (Pal) or octanoylcarnitine (Oct) (10 or 20 μM , respectively, if not stated otherwise) to measure FAO-dependent OXPHOS capacity (F (N)-pathway)¹⁸. In one group, acylcarnitine was substituted by the carrier, H₂O. Cytochrome *c* 10 μM was added to test the integrity of the mitochondrial outer membrane (mtOM). Further titrations with malate (final concentrations of 0.2, 0.5, 1.0, and 2.0 mM) were performed, and pyruvate 5 mM was added supporting NADH-linked respiration (FN-pathway). Glutamate 10 mM was added as an additional substrate for the N-pathway. Succinate (10 mM and later 50 mM final concentration) was added to reconstitute convergent respiration through the FNS-pathway. Glycerophosphate 10 mM was added to support glycerophosphate dehydrogenase Complex-linked respiration (FNSGp-pathway). Stepwise titrations (0.5 μM) of the uncoupler carbonyl cyanide *m*-chlorophenyl hydrazine (CCCP) were performed to determine the electron transfer (ET) capacity at optimum uncoupler concentration. Rotenone 0.5 μM , a CI inhibitor, was added to determine the SGp-pathway ET capacity. Finally, antimycin A 2.5 μM , a CIII inhibitor, was titrated to determine residual oxygen consumption (*Rox*), which was used to correct all respiratory rates.

To evaluate the optimal concentration of acylcarnitine, after titration of ADP 5 mM and malate 0.1 mM, increasing concentrations of palmitoylcarnitine or octanoylcarnitine were titrated (with final concentrations of 10, 20, and 50 μM), followed by cytochrome *c* 10 μM , malate 2 mM, pyruvate 5 mM, glutamate 10 mM, succinate 10 mM, rotenone 0.5 mM and antimycin A 2.5 μM (SUIT-041).

For experiments comparing different mouse tissues, the brains of different species, and the MCAO and aging models, a shortened version of the protocol was used with the following sequential titrations: ADP 5 mM; malate 0.1 mM; carnitine 100 μM ; palmitoylcarnitine 10 μM , malate 2 mM, pyruvate 5 mM, glutamate 10 mM, succinate 10 mM, uncoupler (CCCP) up to the optimum concentration (highest O₂ flux); rotenone 0.5 μM ; and antimycin A 1.5 μM (SUIT-039). To compare brain substructures, a variation of this protocol was used, with the addition of glycerophosphate 10 mM before or after succinate (SUIT-040).

To determine the contribution of each substrate to the respiratory rate, the flux control efficiency (J_{Z-Y}) was calculated (Equation 1)¹²:

$$J_{Z-Y} = 1 - Y_X/Z_X, \quad (1)$$

where Z_X is the reference state with high (stimulated or uninhibited) flux and Y_X is the background state at low flux, upon which the metabolic control variable, X, acts. This allowed to analyze whether the presence of the acylcarnitines impacted the next measurements of the protocol, the flux control efficiencies of the FN-, FNS-, FNSGp- and SGp-pathways.

2.6. Statistical analysis

All results are expressed as the mean \pm standard deviation (SD). Student's *t* test, one-way ANOVA, or two-way ANOVA was used depending on the number of groups, as stated in the figure legends, *p* values are described in the figures or tables in supplementary

material. The statistical calculations were performed using the GraphPad Prism 10.0 software package (GraphPad Software, Inc., La Jolla, California, USA).

Flux control ratios were calculated for all brain regions studied as the slope of an inverted linear regression with zero intercept³⁵.

3. Results

3.1. A high-resolution respirometry protocol to analyze fatty acid oxidation in brain tissues

FAO of mouse brain was compared using octanoylcarnitine and palmitoylcarnitine as MC and LC acylcarnitines. The F-OXPHOS capacity was calculated by subtracting the O₂ flux after the low concentration of malate from the O₂ flux after titration of FAO substrates:

$$\text{F-OXPHOS capacity} = J_{\text{FA}} - J_{\text{M0.1}} \quad (2)$$

The optimum concentration for maximum O₂ flux was 20 μM of octanoylcarnitine, and 10 μM of palmitoylcarnitine. The maximum O₂ flux with palmitoylcarnitine was 4 times higher than with octanoylcarnitine. However, 20-50 μM palmitoylcarnitine inhibited respiration (Figure 1). Optimal concentrations were used in further experiments.

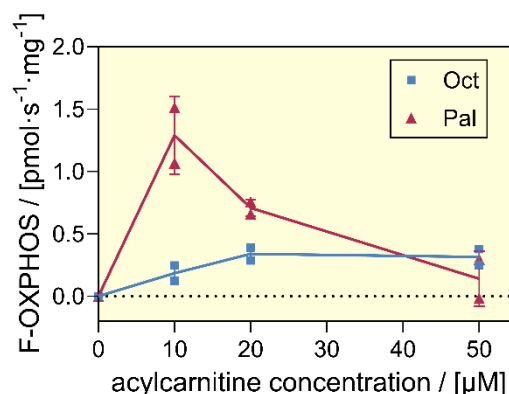


Figure 1. Optimal concentrations of acylcarnitines for fatty acid oxidation (FAO) F-OXPHOS capacity of mouse brain homogenate. Octanoylcarnitine (Oct, squares) or palmitoylcarnitine (Pal, triangles) were titrated stepwise in the presence of ADP 5 mM and malate 0.1 mM. The F-OXPHOS capacity was normalized by tissue wet mass and calculated from the O₂ flux after each acylcarnitine titration, J_{FA} , subtracting the preceding O₂ flux in the absence of acylcarnitine, $J_{\text{M0.1}}$. Average \pm SD; $N=2$ mice, measured in duplicate, $n=2$.

Figure 2a shows a representative trace of the SUIT protocol used to compare F-OXPHOS capacity (F_P) with respiration stimulated by sequentia titrations of NADH-linked substrates (FN_P), succinate (FNS_P), glycerophosphate (FNSG_P), followed by uncoupler titrations to determine the ET capacity (FNSG_P). Figure 2b is a zoom into the section of the F(N)-pathways to visualize the increase in O₂ flux after palmitoylcarnitine titration.

The same protocol was applied with palmitoylcarnitine and octanoylcarnitine and the carrier H₂O as a control, expressing O₂ flux per wet tissue mass (Figure 3a and 3b). The F-OXPHOS capacity with palmitoylcarnitine was higher than with octanoylcarnitine (Figure 3c), consistent with the previous experiment (Figure 1). Palmitoylcarnitine but not octanoylcarnitine inhibited OXPHOS capacity supported by pyruvate as shown by the

flux control efficiencies (Figure 3d). Glutamate feeds into the TCA cycle and generates NADH in the mitochondrial matrix, independent of pyruvate. The fact that glutamate restored N-pathway OXPHOS capacity in the presence of palmitoylcarnitine points to an inhibitory effect of palmitoylcarnitine specifically on pyruvate oxidation. Both acylcarnitines did not exert a disruptive effect on the mtOM, as shown by unchanged cytochrome *c* flux control efficiencies (Figure S1).

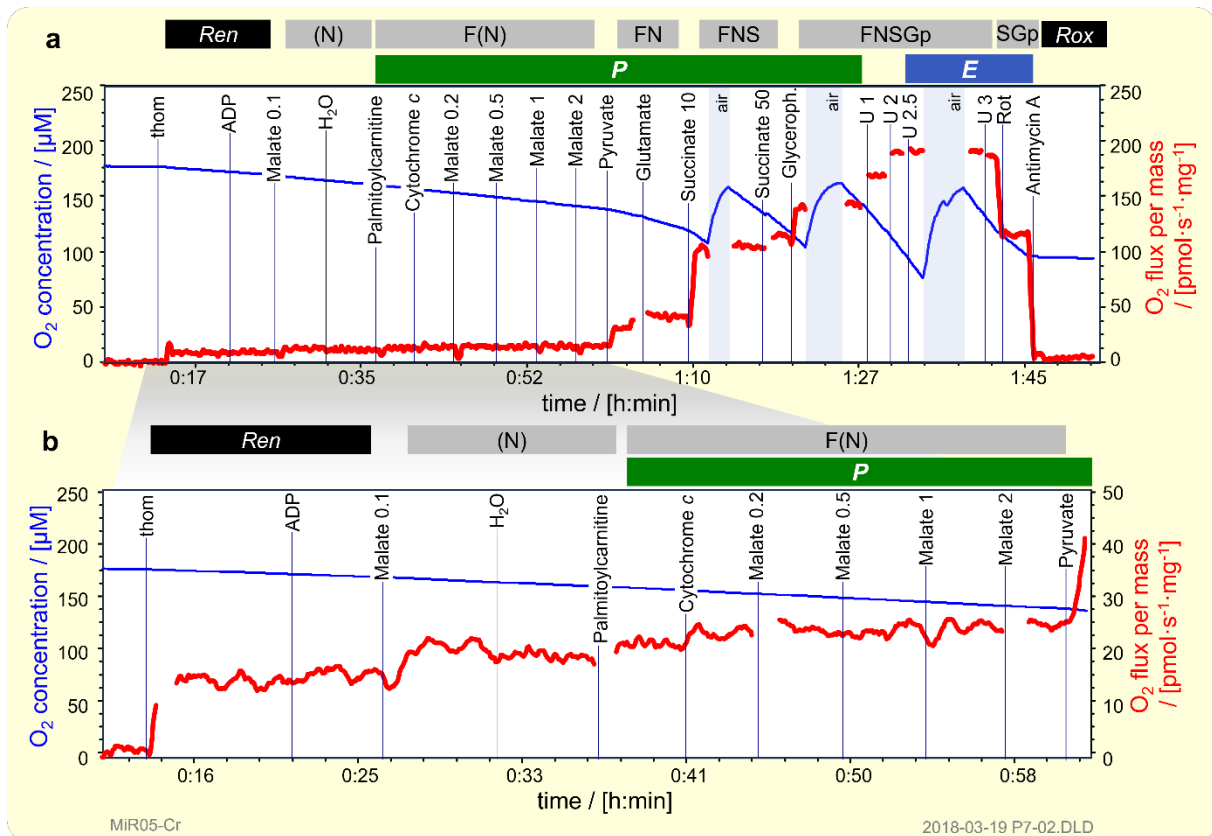


Figure 2. High-resolution respirometry with substrate-uncoupler-inhibitor-titration (SUIT) protocol for measuring fatty acid oxidation (F-OXPHOS capacity) and malate kinetics. Representative traces with mouse brain homogenate. The blue line shows the O₂ concentration in the chamber, while the red line depicts the O₂ flux per protein concentration. Sections of OXPHOS capacity, *P*, and electron transfer (ET) capacity, *E*, are indicated by green and blue bars, respectively. Residual endogenous respiration (*Ren*) and residual oxygen consumption (*Rox*) are shown by black bars. **(a)** Electron-transfer pathway states are marked by gray bars, where F, N, S and Gp indicate fatty acid oxidation-, NADH-, succinate-, and glycerophosphate-linked respiration, respectively. Titrations are indicated by vertical lines: tissue homogenate thom; ADP 5 mM; cytochrome *c* 10 μM; malate (concentrations indicated in mM); pyruvate 5 mM; glutamate 10 mM; succinate (concentrations in mM); uncoupler U (concentrations in μM); rotenone 0.5 μM Rot and antimycin A 2.5 μM. **(b)** Magnified view from panel (a) highlighting FAO-related O₂ flux.

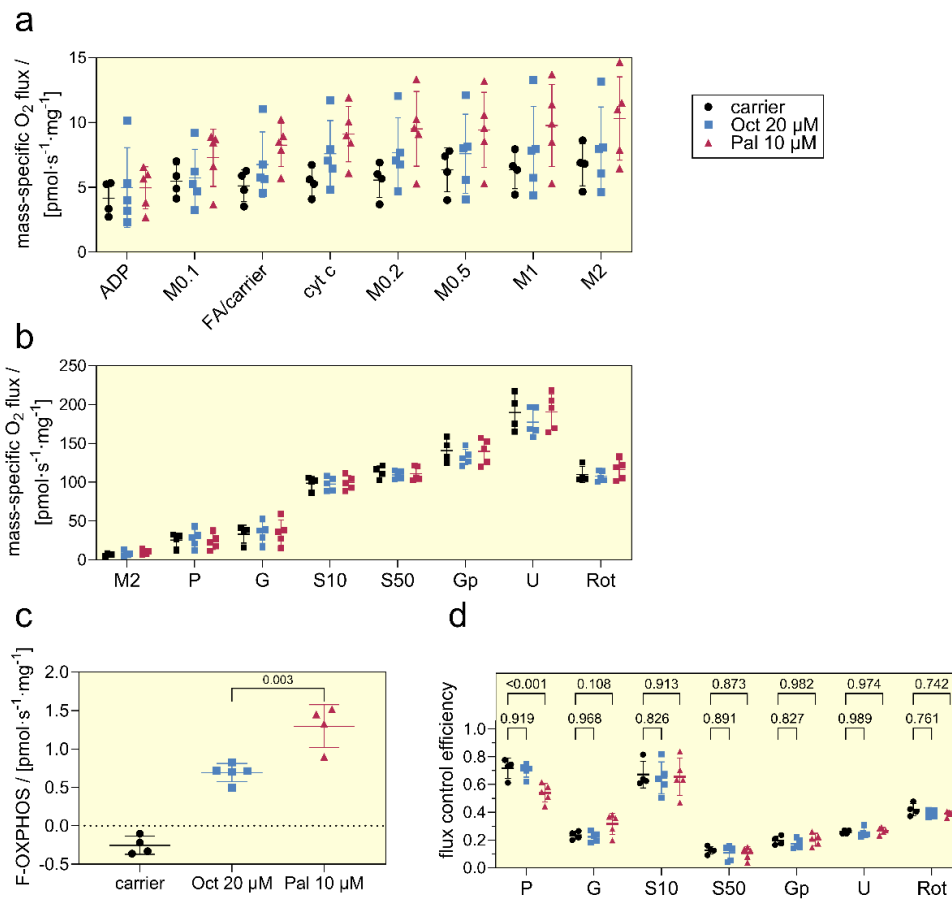


Figure 3. OXPHOS and ET capacities including fatty acid oxidation (FAO) in mouse brain homogenates. O₂ flux per tissue mass, corrected for residual oxygen consumption measured in the presence of the CIII inhibitor antimycin A. **(a)** First part of the protocol (Fig. 2b), titration sequence: ADP; malate 0.1 mM, M0.1, acylcarnitine or carrier (H₂O) as indicated in the box (carrier, circle; octanoylcarnitine, square; palmitoylcarnitine, triangle); cytochrome *c*; and malate from 0.2 to 2 mM, M0.2 to M2. **(b)** Second part of the experiment (Fig. 2a), titration sequence: malate M2; pyruvate P; glutamate, G; succinate S (10 and then 50 mM); glycerophosphate Gp; and rotenone, Rot. **(c)** F-OXPHOS capacity using the optimal concentrations of octanoylcarnitine (Oct, 20 μM) or palmitoylcarnitine (Pal, 10 μM) compared to carrier (H₂O). **(d)** Flux control efficiencies in the presence or absence of acylcarnitines. Mean ± SD of 4–5 independent measurements. Two-way ANOVA was used for the statistics in (d); unpaired Student's *t* test was used in (c), *p* values are shown.

Malate kinetics: In the presence of ADP, cytochrome *c*, and absence of fuel substrates (carrier H₂O as a control for acylcarnitines), titration of malate from 0.1 to 2 mM increased respiration in mouse brain homogenate (Figure 4a). This indicates the activity of the FAO-independent malate-anaplerotic pathway. Subtracting these control rates at each malate concentration from the malate kinetics in the presence of palmitoylcarnitine or octanoylcarnitine revealed that maximum F-OXPHOS capacities were obtained at a kinetically saturating concentration of 0.1 mM malate (Figure 4b). This provided the rationale for a slightly simplified SUIT protocol with a malate concentration of 0.1 mM for measurement of FAO capacity. However, N-pathway capacity required kinetically a higher malate concentration of 2 mM.

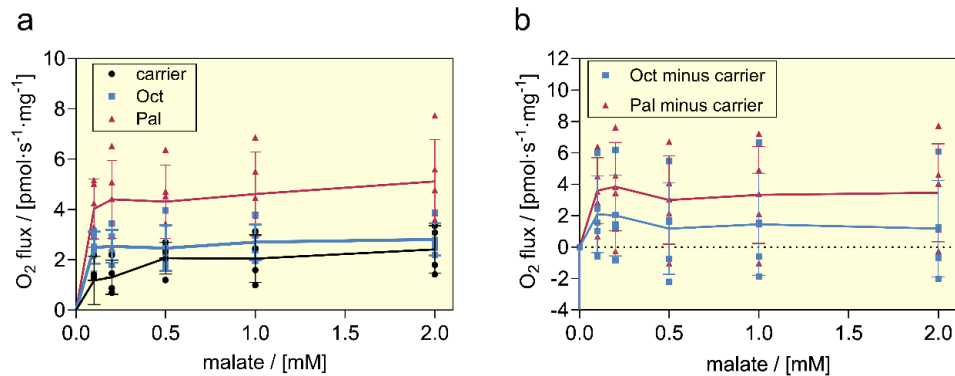


Figure 4. Malate kinetics in the absence and presence of acylcarnitines. Sequential titrations of malate in the presence of ADP and cytochrome *c*. O₂ flux per mass of wet tissue. **(a)** O₂ flux after subtraction of the initial O₂ flux at zero malate concentration. **(b)** O₂ flux additionally corrected by the means of the carrier group at each malate concentration. Means \pm SD, *N*=4.

3.2 FAO in different mouse tissues

As expected, F-OXPHOS capacity was highest in the heart, lowest in brain (45 times lower), and intermediate in kidney (3.5 times lower than in the heart) (Figure 5a).

To compare the contribution of FAO to the overall energy metabolism of the different tissues, F-OXPHOS capacities were normalized for FN-OXPHOS capacity (Figure 5b) or FNS-OXPHOS capacity. F-OXPHOS/FNS-OXPHOS in the brain was approximately 15 times lower than that in the heart, while in the kidney it was 2.3 times lower (Figure 5c). Since these tissues have high aerobic capacity and mitochondrial content, the patterns of mass-specific F-OXPHOS capacity and flux control ratios remained similar.

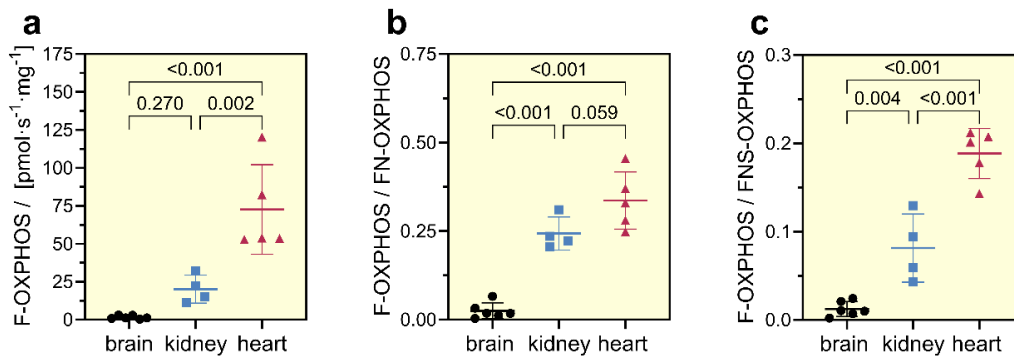


Figure 5. Fatty acid oxidation (FAO) capacity in mouse brain, kidney and heart tissues. **(a)** F-OXPHOS capacity calculated according to equation 2. Internal normalization of F-OXPHOS capacity using **(b)** FN-OXPHOS and **(c)** FNS-OXPHOS as the reference state. Flux control ratios were calculated intraexperimentally as F-OXPHOS capacity/O₂ flux with FN or FNS pathway substrates, PalPGM_P and PalPGMS_P, respectively (palmitoylcarnitine, pyruvate, glutamate, malate and succinate). Means \pm SD, *N*=4–6. One-way ANOVA followed by Tukey's test; *p* values are shown.

3.2 FAO in different mouse brain regions

In mouse brain, the cerebellum had the highest F-OXPHOS capacity, followed by the hypothalamus, cortex, and prefrontal cortex. In the hippocampus, F-OXPHOS capacity was practically undetectable (Figure 6a). Similarly, FN- and FNSGp-OXPHOS were highest in the cerebellum. FN_P increased linearly and proportionally with $FNSGp_P$, which indicates a constant flux control ratio calculated as the slope of 0.59 in these regions of the brain (Figure 6b, Figure S2a and S2b). SGP-ET capacity, measured after titration of uncoupler and rotenone, was likewise linearly related to FNSGp-ET capacity, with a flux control ratio of 0.36 (Figure 6c, S2c and S2d). The FNSGp P/E ratio was 0.74, as calculated from the slope $FNSGp_P / FNSGp_E$, with a similar correlation coefficient $r^2 = 0.94$ (or 0.98 with intercept forced through zero), in contrast to the mouse heart with an NS P/E ratio close to one³⁶.

F-OXPHOS capacity was measured at a low malate concentration (0.1 mM) and corrected for O_2 flux before titration of Pal. Uncorrected (total) respiration measured at 2 mM malate did not correlate with F-OXPHOS capacity ($r^2 = 0.13$). Malate anaplerosis-enhanced respiration interferes with the quantification of FAO at high malate concentrations. We calculated the malate anaplerosis-enhanced respiration as the sum of the step increases in respiration upon titration of 0.1 mM (before Pal) and 2 mM malate (after Pal). This is based on the assumption that the malate anaplerosis with 2 mM malate exerts an additive effect on F-OXPHOS, as justified by the results in Figure 4. This malate anaplerosis enhanced respiration correlated with FN-OXPHOS capacity (Figure 6d, Figure S2g).

A linear pattern as observed in Figures 6b-d suggests quantitative but no qualitative changes in mitochondrial respiratory control patterns between brain regions. In contrast, however, F-OXPHOS capacity did not follow the same pattern (Figure 6e). The FAO/FN flux control ratio was highest for the hypothalamus (Figure S2c). Altogether, this indicates that mitochondria in different brain regions are qualitatively different. The large scatter indicates variability between regions and between individual mice.

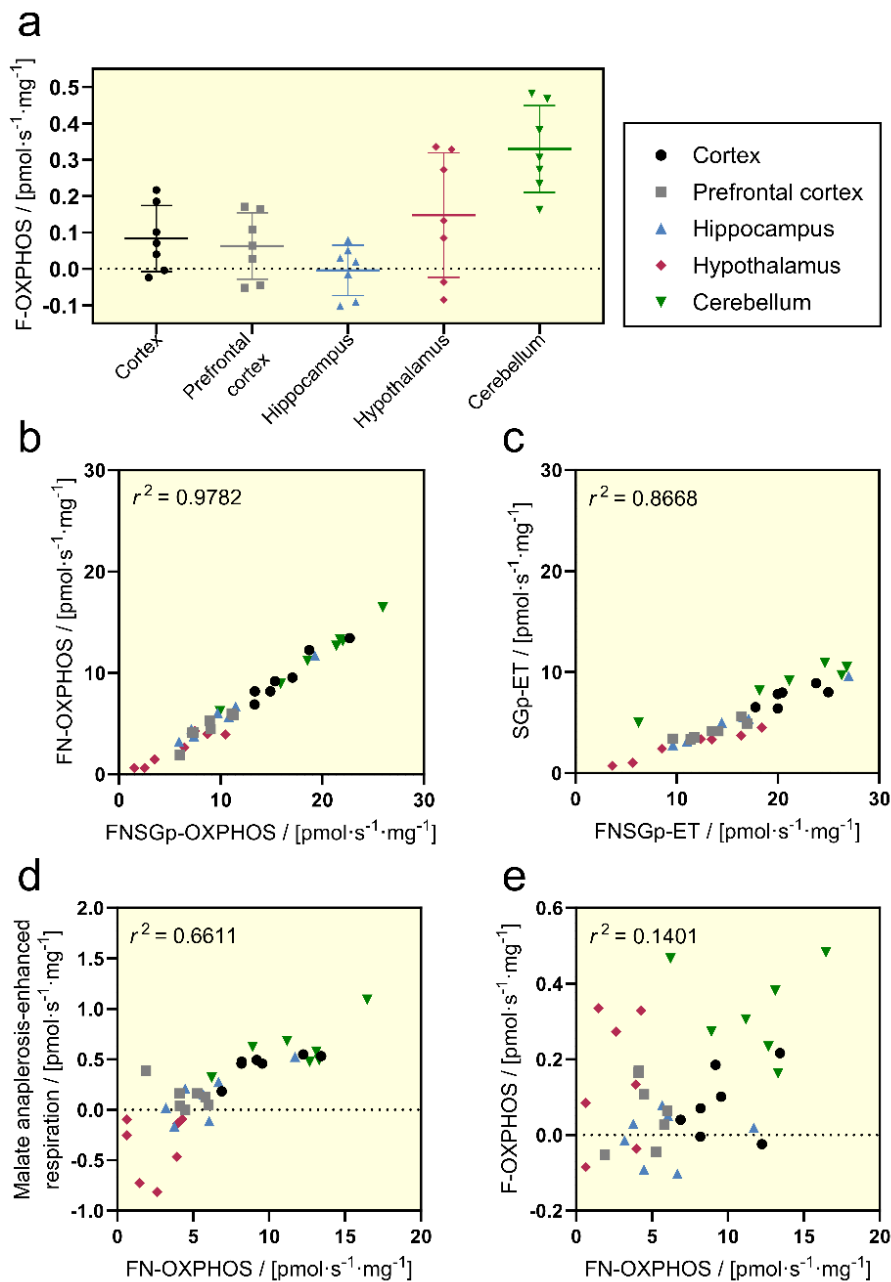


Figure 6. Respiration of mouse brain regions (cortex, prefrontal cortex, hippocampus, hypothalamus, and cerebellum) normalized per tissue protein. (a) F-OXPPOS capacity in the presence of $10\ \mu\text{M}$ palmitoylcarnitine (Pal), $0.1\ \text{mM}$ malate, and ADP, means \pm SD, Tukey's test following one-way ANOVA. *p* values are shown in Table S1. **(b)** FN-OXPPOS capacity (Pal, pyruvate, glutamate, malate) compared to FNSGp-OXPPOS capacity (same substrates plus succinate and glycerophosphate). **(c)** SGp-ET capacity (after titration of rotenone) compared to FNSGp-ET capacity (after uncoupler titration). **(d)** Malate-anaplerotic respiration (the sum of increases in respiration after titration of $0.1\ \text{mM}$ malate at $5\ \text{mM}$ ADP and titration of $2\ \text{mM}$ malate after addition of Pal and cytochrome *c*), compared to FN-OXPPOS capacity. **(e)** F-OXPPOS capacity compared to FN-OXPPOS capacity. $N=6$, other results are shown in Figure S2. r^2 from linear regression without forcing the intercept through zero.

3.2 FAO in different animal species

Furthermore, we compared the F-OXPHOS capacity in the brains of two homeothermic mammalian species, mice (C57bl/6 N) and rats (Wistar) measured at 37 °C, with the heterothermic insect *Drosophila melanogaster*, measured at 25 °C. The average F-OXPHOS capacity expressed per tissue wet mass was similar in mice and rats with high variability for mice (Figure 7a). The F-OXPHOS-capacity per tissue wet mass in the *Drosophila* brain was markedly lower than that in the mouse and rat brains, without adjustment for the experimental temperature. To achieve comparability, respiratory rates were normalized for rates in the reference states FN- and FNS-OXPHOS. This revealed that actually the FAO in *Drosophila* brain was relatively higher than in rodents (Figure 7b and 7c).

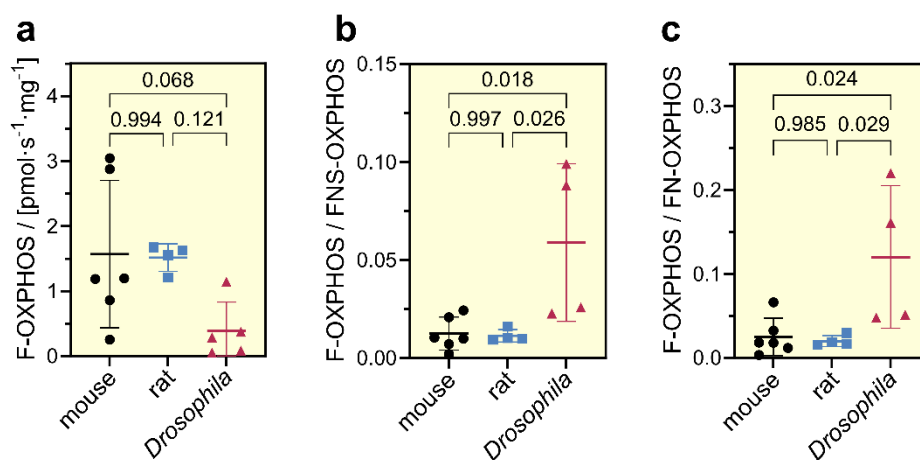


Figure 7. Brain fatty acid oxidation (FAO) in mouse, rat and *Drosophila*. (a) F-OXPHOS capacity in brain tissues normalized by wet tissue mass. (b) and (c) Intraexperimental ratios of F-OXPHOS capacity per O₂ flux in the FNS- or FN-pathway, with substrates PalPGMS or PalPGM, respectively (palmitoylcarnitine, pyruvate, glutamate, malate and succinate). Mean ± SD, N=4–6. One-way ANOVA followed by Tukey's test; *p* values are shown.

3.2. FAO in ischemic brain

To evaluate the effect of ischemia on F-OXPHOS capacity in brain, endothelin-1 (ET-1)-induced brain ischemia was studied as a model. Mitochondrial respiration in non-risk and stroke-affected areas of the rat brain was measured after 2 and 24 h of the stroke induction. In comparison to sham animals and non-risk areas, the risk area of the brain exhibited a trend of decreasing F-OXPHOS capacity (Figure 8a; *p* values summarized in Table S2). Moreover, a similar trend was observed in the FNS-OXPHOS rate in the risk area 24 hours after the induction of ischemia (Figure 8b). However, F-OXPHOS capacity declined even when normalized for FN- and FNS-OXPHOS (Figure 8c and 8d). This indicates that FAO is a highly sensitive and specific target of mitochondrial ischemic injury. Since acylcarnitine content is a marker of mitochondrial FAO, we determined the acylcarnitine profile in the brain. Ischemia increased the levels of MC and LC acylcarnitines in the risk area 24 h after ET-1 administration (Figures 8e and 8f).

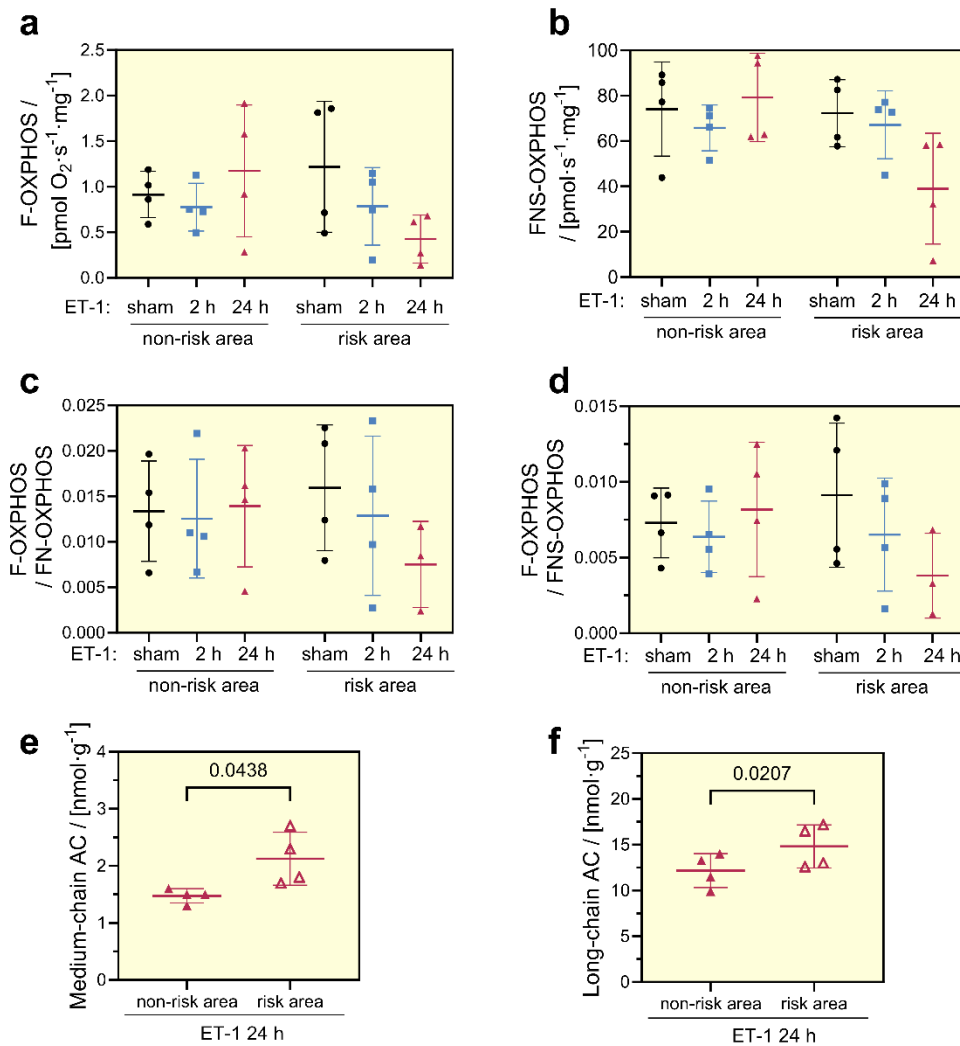


Figure 8. Rat brain fatty acid oxidation (FAO), FNS-OXPHOS capacity and acylcarnitine levels in an ischemia model. Rats were submitted to endothelin-1 (ET-1) or saline (sham) brain injection. The brains were collected 2 h or 24 h after ET-1 injection. Risk areas and non-risk areas were compared. **(a)** F-OXPHOS capacity in the presence of palmitoylcarnitine (Pal) 10 μ M, malate 0.1 mM, and ADP, corrected for the O₂ flux prior to Pal titration. **(b)** FNS-OXPHOS capacity, measured in the presence of ADP, Pal, pyruvate, glutamate, malate, and succinate. **(c)** and **(d)** Intraexperimental ratios between F-OXPHOS capacity and O₂ flux with FN- or FNSGp-pathway substrates, PalPGM or PalPGMSGp respectively (palmitoylcarnitine, pyruvate, glutamate, malate, succinate, glycerophosphate). Comparison of medium-chain and **(e)** long-chain acylcarnitine content **(f)**. Mean \pm SD of 3–4 animals. Two-way ANOVA followed by Tukey's test (a, b, c, d), *p*-values are shown in Table S2; paired Student's *t* test (e, f).

3.3. FAO in aging brain

In the rat aging model, the F-OXPHOS capacity was 2-fold lower in the brain of rats aged 20 months compared to adult animals (8 months) (Figure 9a). In contrast, brain FNS-OXPHOS capacity was not different between adult and old rats (Figure 9b). Accordingly, F-OXPHOS capacity normalized for FN- and FNS-OXPHOS was lower in the old rats (Figure 9c and 9d). Furthermore, the content of LC acylcarnitines was increased in the old animals (Figure 9e). No changes were observed in MC acylcarnitine content in the brain due to aging (Figure 9f).

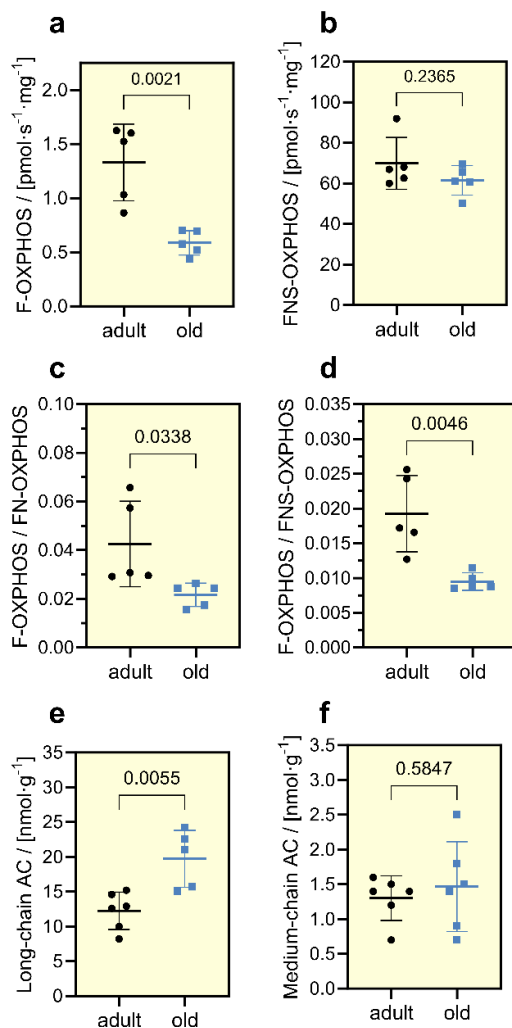


Figure 9. Effect of age on brain fatty acid oxidation in rat. Adult (8 months) and old (20 months) rats. **(a)** F-OXPHOS capacity, in the presence of palmitoylcarnitine (Pal) 10 μ M, malate 0.1 mM and ADP, corrected for the O_2 flux prior to Pal titration. **(b)** FNS-OXPHOS capacity in the presence of Pal, pyruvate, glutamate, 2 mM malate, succinate and ADP. **(c)** and **(d)** Intraexperimental ratios between F-OXPHOS capacity and O_2 flux with FN- or FNSGp-pathway substrates, PalPGM or PalPGMSGp respectively (palmitoylcarnitine, pyruvate, glutamate, malate, succinate, glycerophosphate). **(e)** Long- and **(f)** medium-chain acylcarnitine content. Mean \pm SD, $N=5$. Unpaired Student's t test; p values are shown.

4. Discussion

The study of fatty acid oxidation addresses the most complex metabolic pathway of mitochondrial core energy metabolism¹². Octanoate or octanoylcarnitine are widely used as a substrate of FA-linked respiration. However, different pathways participate in the metabolism of long-chain (LC) and medium-chain (MC) FAO³⁷. Therefore, respiration on octanoylcarnitine as a substrate does not represent overall FA metabolism in mitochondria. Octanoate and other MCFAs enter mitochondria without the carnitine-dependent CPT1/CPT2 and carnitine/acylcarnitine translocase system⁶. Thus, MCFA metabolism is considered faster and is not inhibited by malonyl-CoA. MCFAs have been

proposed as a treatment to compensate for LCFAO defects¹⁹. However, it was shown that in heart and skeletal muscle, oxidation of MCFAs depends on the carnitine-mediated FA transfer system, in contrast to liver. Accordingly, octanoate failed to compensate for CPT2 deficiency in mice³⁸.

Octanoate contributes up to 20 % to metabolism in rat brain². LC and MC acylcarnitine metabolism in the brain has not been compared in previous studies. In human heart, octanoylcarnitine exerted an additive effect on F-OXPHOS capacity with palmitoylcarnitine and malate³⁹. Lauroylcarnitine (C12) supports the highest F-pathway respiration in rat heart and skeletal muscle (gastrocnemius), closely followed by decanoylcarnitine (C10) and myristoylcarnitine (C14), when tested at 20 μM acylcarnitine concentration⁴⁰. In our study, using optimal concentrations of octanoylcarnitine (20 μM) and palmitoylcarnitine (10 μM), LC acylcarnitine oxidation was 4 times higher than MC acylcarnitine (Figure 1). Notably, the LC acylcarnitine concentration in the brain reached 12 μM (Figure 8f, Figure 9e), which is comparable to that in skeletal muscle and heart²⁸, while the concentration of MC acylcarnitines was approximately 10 times lower in brain (Figure 8e, Figure 9f). Accordingly, 10 μM palmitoylcarnitine used in measurements of mitochondrial respiration corresponds to physiological concentrations of LC acylcarnitines in the brain. In contrast, the 20 μM octanoylcarnitine concentration exceeds the physiological level of MC acylcarnitines in the brain by approximately 15-fold. Taken together, it is important to use a variety of MC and LCFAs or acylcarnitines as substrates for the characterization of mitochondrial FAO.

Malate is required as a cosubstrate to study FAO to avoid acetyl-CoA accumulation with consecutive inhibition of FAO^{12,17}. Typically, malate alone does not support mitochondrial respiration if oxaloacetate is not further metabolized in the absence of acetyl-CoA. However, when mitochondrial malic enzyme is present, the malate-anaplerotic pathway generates pyruvate and the TCA cycle is refueled, with NADH production independent of FAO. This stimulation of respiration through the N-pathway must be avoided for estimating FAO capacities.

Mitochondrial malic enzyme is expressed in rat and human brain^{41,42}. Different mouse strains present variable mt-malic enzyme activity⁴³. McKenna et al.⁴⁴ observed higher malic enzyme activity in mitochondria from cortical synaptic terminals than in mitochondria from primary cultures of cortical neurons or cerebellar granule cells. We tested the possible impact of mitochondrial malic enzyme on FAO assessment in the mouse brain by employing kinetics with malate titrations from 0.1 to 2 mM. 0.1 mM malate saturated F-OXPHOS capacity in mouse brain (Figure 4). A further increase in malate concentration, however, activated malate anaplerosis, leading to overestimation of FAO capacity.

Studies performed using high concentrations of malate for FAO assessment in the brain must thus be interpreted with care. Overestimation of FAO is avoided by baseline correction of respiration at low malate concentrations: F-OXPHOS capacity is calculated as the difference in O_2 flux before and after addition of acylcarnitine. This correction is essential for analysis in brain mitochondria, with FAO capacity as low as 1 % of carbohydrate-linked NS-OXPHOS capacity. Respiration due to malate anaplerosis was higher in the cerebellum than in the cortex and prefrontal cortex, while it was absent in the hippocampus and hypothalamus (Figures 6 and S2).

Respiratory N- and S-pathway capacities differ between brainstem, hippocampus, motor cortex and striatum³⁴. We extended this study by showing an even more

pronounced region-specific variety of FAO capacity. F-OXPHOS capacity was highest in the cerebellum, followed by the hypothalamus, and almost no FAO activity in hippocampus (Figure 6a). The F-OXPHOS capacities did not correlate with FN-OXPHOS (Figure 6e) thus indicating N-pathway independent variability of FAO in different brain regions: Cortex and prefrontal cortex showed similar F-OXPHOS capacity, but cortex showed higher FN-, FNSGp-OXPHOS and SGp-ET capacities than prefrontal cortex (Figures 6a, 6e, and S2).

FAO capacity depends on the expression of CPT enzymes that together with CAT ensure LCFA transfer into mitochondria³. In a previous study, the highest CPT2 enzyme expression was found in the cerebellum, in agreement with our results³. Opposite to our results, however, the same study demonstrated a higher oleate oxidation rate in the hippocampus than in the cortex.

In our study, FAO had a higher contribution to brain energy metabolism in *Drosophila* than in rodents (Figure 7), consistent with the specific metabolic relevance of FAO in *Drosophila* brain^{45,46}.

Our results confirm that FAO occurs in brain tissue but has lower relevance as a bioenergetic pathway compared to kidney and heart (Figure 5). However, acylcarnitine content in the brain (Figures 7 and 8) is comparable to that in other tissues²⁸, suggesting specific metabolic roles for FAO in the brain, which opens paths for further investigation.

The role of acylcarnitines in the pathogenesis of central nervous system disorders receives increasing attention⁶. High concentrations of LC acylcarnitines in tissues and blood are markers of mitochondrial dysfunction⁶. In our study, low mitochondrial FAO capacity in the area of stroke and in the brain of aged rats correlated with high levels of acylcarnitines. This is in line with previous observations that LC acylcarnitine levels are elevated in brain of aged mice and a stroke model²⁴. Alterations in acylcarnitine concentrations have been reported from clinical trials on neurodegenerative and psychiatric disorders such as Alzheimer's disease⁴⁷, cognitive decline⁴⁸, Parkinson's disease⁴⁹, depression⁵⁰, schizophrenia⁵¹ and psychosis⁵². In a patient cohort of traumatic brain injury with intracranial injury, higher total acylcarnitine levels in serum were associated with poor functional outcomes after injury⁵³. However, it remains largely unknown whether acylcarnitine levels in the circulation correspond to acylcarnitine levels in brain tissues and whether such associations provide diagnostic information on mitochondrial energy metabolism in the brain.

In conclusion, FAO deserves attention in studies of brain metabolism. The protocols described allow for quantitative measurement of F-OXPHOS capacity in brain, and other tissues with low F-OXPHOS capacity and malate anaplerosis. Palmitoylcarnitine is the preferable substrate of FAO compared to octanoylcarnitine in the brain, but additive effects exerted by combinations of different acylcarnitines need to be evaluated further.

Funding: The authors were funded by the European Union's Horizon 2020 research and innovation programme, grant number 857394.

Ethics approval statement: The animal study protocols were approved by the Institutional Review Board Ethics Council of Animal Protection at the Veterinary and Food Service, Riga, Latvia (ethical approvals No. 82 and 83) or were conducted in accordance with the Austrian Animal Experimentation Act (Tierversuchsgesetz 2012; Directive 2010/63/EU; BMWFM-66.011/0128-WF/V/3b/2016).

Abbreviations

CAT	Carnitine acylcarnitine translocase	LC	Long chain
CoA	Coenzyme A	MC	Medium chain
CoQ	Coenzyme Q	Oct	Octanoylcarnitine
CPT	Carnitine palmitoyltransferase	Pal	Palmitoylcarnitine
FA	Fatty acid	SC	Short chain
FAO	Fatty acid oxidation		

References

- Allweis C, Landau T, Abeles M, Magnes J. The oxidation of uniformly labelled albumin-bound palmitic acid to CO₂ by the perfused cat brain. *J Neurochem.* 1966;13(9):795–804.
- Ebert D, Haller RG, Walton ME. Energy contribution of octanoate to intact rat brain metabolism measured by ¹³C nuclear magnetic resonance spectroscopy. *J Neurosci.* 2003;23(13):5928–5935.
- Jernberg JN, Bowman CE, Wolfgang MJ, Scafidi S. Developmental regulation and localization of carnitine palmitoyltransferases (CPTs) in rat brain. *J Neurochem.* 2017;142(3):407–419.
- Morant-Ferrando B, Jimenez-Blasco D, Alonso-Batan P et al. Fatty acid oxidation organizes mitochondrial supercomplexes to sustain astrocytic ROS and cognition. *Nat Metab.* 2023;5(8):1290–1302.
- Popov A, Brazhe N, Fedotova A et al. A high-fat diet changes astrocytic metabolism to promote synaptic plasticity and behavior. *Acta Physiologica.* 2022;236(1):e13847.
- Dambrova M, Makrecka-Kuka M, Kuka J et al. Acylcarnitines: Nomenclature, Biomarkers, Therapeutic Potential, Drug Targets, and Clinical Trials. *Pharmacol Rev.* 2022;74(3):506–551.
- Roberts DL, Frerman FE, Kim JJ. Three-dimensional structure of human electron transfer flavoprotein to 2.1-Å resolution. *Proc Natl Acad Sci U S A.* 1996;93(25):14355–14360.
- Crane FL, Beinert H. On the mechanism of dehydrogenation of fatty acyl derivatives of coenzyme A. II. The electron-transferring flavoprotein. *J Biol Chem.* 1956;218(2):717–731.
- Ramsay RR, Steenkamp DJ, Husain M. Reactions of electron-transfer flavoprotein and electron-transfer flavoprotein: ubiquinone oxidoreductase. *Biochem J.* 1987;241(3):883–892.
- Ruzicka FJ, Beinert H. A new iron-sulfur flavoprotein of the respiratory chain. A component of the fatty acid beta oxidation pathway. *J Biol Chem.* 1977;252(23):8440–8445.
- Zhang J, Frerman FE, Kim J-JP. Structure of electron transfer flavoprotein-ubiquinone oxidoreductase and electron transfer to the mitochondrial ubiquinone pool. *Proc Natl Acad Sci U S A.* 2006;103(44):16212–16217.
- Gnaiger E. Mitochondrial Pathways and Respiratory Control An Introduction to OXPHOS Analysis. *Bioenerg Commun.* 2020.2:1–112. doi: 10.26124/bec:2020-0002
- Gnaiger E. Complex II ambiguities – FADH₂ in the electron transfer system. *J Biol Chem* - in press.
- Komlódi T, Cardoso LHD, Doerrier C, Moore AL, Rich P, Gnaiger E. Coupling and pathway control of coenzyme Q redox state and respiration in isolated mitochondria. *Bioenerg Commun.* 2021.3:1–28. doi: 10.26124/bec:2021-0003
- Gnaiger E, MitoEAGLE Task Group. Mitochondrial physiology. *Bioenerg Commun.* 2020.1:1–44. doi: 10.26124/bec:2020-0001.v1.
- Carpenter K, Pollitt RJ, Middleton B. Human liver long-chain 3-hydroxyacyl-coenzyme A dehydrogenase is a multifunctional membrane-bound beta-oxidation enzyme of mitochondria. *Biochem Biophys Res Commun.* 1992;183(2):443–448.

- 17 Ojuka E, Andrew B, Bezuidenhout N et al. Measurement of β -oxidation capacity of biological samples by respirometry: a review of principles and substrates. *American Journal of Physiology-Endocrinology and Metabolism*. 2016;310(9):E715–E723.
- 18 Doerrier C, Garcia-Souza LF, Krumschnabel G, Wohlfarter Y, Mészáros AT, Gnaiger E. High-Resolution FluoRespirometry and OXPHOS Protocols for Human Cells, Permeabilized Fibers from Small Biopsies of Muscle, and Isolated Mitochondria. *Methods Mol Biol*. 2018;1782:31–70.
- 19 Schönfeld P, Wojtczak L. Short- and medium-chain fatty acids in energy metabolism: the cellular perspective. *J Lipid Res*. 2016;57(6):943–954.
- 20 Kerner J, Hoppel C. Fatty acid import into mitochondria. *Biochim Biophys Acta*. 2000;1486(1):1–17.
- 21 Barber CN, Raben DM. Lipid Metabolism Crosstalk in the Brain: Glia and Neurons. *Front Cell Neurosci*. 2019;13:212.
- 22 Magistretti PJ, Allaman I. A cellular perspective on brain energy metabolism and functional imaging. *Neuron*. 2015;86(4):883–901.
- 23 McCann MR, George De la Rosa MV, Rosania GR, Stringer KA. L-Carnitine and Acylcarnitines: Mitochondrial Biomarkers for Precision Medicine. *Metabolites*. 2021;11(1). doi:10.3390/metabo11010051.
- 24 Mavroudakis L, Lanekoff I. Ischemic Stroke Causes Disruptions in the Carnitine Shuttle System. *Metabolites*. 2023;13(2). doi:10.3390/metabo13020278.
- 25 Vavers E, Zvejniece L, Svalbe B et al. The neuroprotective effects of R-phenibut after focal cerebral ischemia. *Pharmacol Res*. 2016;113:796–801.
- 26 Nikolova S, Moyanova S, Hughes S, Bellyou-Camilleri M, Lee T-Y, Bartha R. Endothelin-1 induced MCAO: dose dependency of cerebral blood flow. *J Neurosci Methods*. 2009;179(1):22–28.
- 27 Liepinsh E, Makrecka-Kuka M, Kuka J et al. Inhibition of L-carnitine biosynthesis and transport by methyl- γ -butyrobetaine decreases fatty acid oxidation and protects against myocardial infarction. *Br J Pharmacol*. 2015;172(5):1319–1332.
- 28 Makrecka-Kuka M, Sevostjanovs E, Vilks K et al. Plasma acylcarnitine concentrations reflect the acylcarnitine profile in cardiac tissues. *Sci Rep*. 2017;7(1):17528.
- 29 Veksler VI, Kuznetsov A V., Sharov VG, Kapelko VI, Saks VA. Mitochondrial respiratory parameters in cardiac tissue: A novel method of assessment by using saponin-skinned fibers. *Biochimica et Biophysica Acta (BBA) - Bioenergetics*. 1987;892(2):191–196.
- 30 Gnaiger E, Kuznetsov A V., Schneeberger S et al. Mitochondria in the Cold. In: Heldmaier G, Klingenspor M (eds). *Life in the Cold*. Springer Berlin Heidelberg: Berlin, Heidelberg, 2000, pp 431–442.
- 31 Lowry OH, Rosebrough NJ, Farr AL, Randall RJ. Protein measurement with the Folin phenol reagent. *J Biol Chem*. 1951;193(1):265–75.
- 32 Makrecka-Kuka M, Volska K, Antone U et al. Trimethylamine N-oxide impairs pyruvate and fatty acid oxidation in cardiac mitochondria. *Toxicol Lett*. 2017;267:32–38.
- 33 Tito AJ, Cheema S, Jiang M, Zhang S. A Simple One-step Dissection Protocol for Whole-mount Preparation of Adult *Drosophila* Brains. *J Vis Exp*. 2016;(118). doi:10.3791/55128.
- 34 Burtscher J, Zangrandi L, Schwarzer C, Gnaiger E. Differences in mitochondrial function in homogenated samples from healthy and epileptic specific brain tissues revealed by high-resolution respirometry. *Mitochondrion*. 2015;25:104–112.
- 35 Gnaiger E. Bioenergetic cluster analysis – mitochondrial respiratory control in human fibroblasts. *MitoFit Preprints*. 2021.7:1–32. doi: 10.26124/mitofit:2021-0008.
- 36 Lemieux H, Blier PU, Gnaiger E. Remodeling pathway control of mitochondrial respiratory capacity by temperature in mouse heart: electron flow through the Q-junction in permeabilized fibers. *Sci Rep*. 2017;7(1):2840.
- 37 Schönfeld P, Reiser G. Brain energy metabolism spurns fatty acids as fuel due to their inherent mitotoxicity and potential capacity to unleash neurodegeneration. *Neurochem Int*. 2017;109:68–77.

- 38 Pereyra AS, Harris KL, Soepriatna AH et al. Octanoate is differentially metabolized in liver and muscle and fails to rescue cardiomyopathy in CPT2 deficiency. *J Lipid Res.* 2021;62:100069.
- 39 Lemieux H, Semsroth S, Antretter H, Höfer D, Gnaiger E. Mitochondrial respiratory control and early defects of oxidative phosphorylation in the failing human heart. *Int J Biochem Cell Biol.* 2011;43(12):1729–1738.
- 40 Fleischman JY, Van den Bergh F, Collins NL, Bowers M, Beard DA, Burant CF. Higher mitochondrial oxidative capacity is the primary molecular differentiator in muscle of rats with high and low intrinsic cardiorespiratory fitness. *Mol Metab.* 2023;76:101793.
- 41 Nagel WO, Dauchy RT, Sauer LA. Mitochondrial malic enzymes. An association between NAD(P)+-dependent malic enzyme and cell renewal in Sprague-Dawley rat tissues. *J Biol Chem.* 1980;255(9):3849–3854.
- 42 Bukato G, Kochan Z, Swierczyński J. Different regulatory properties of the cytosolic and mitochondrial forms of malic enzyme isolated from human brain. *Int J Biochem Cell Biol.* 1995;27(10):1003–1008.
- 43 Bernstine EG, Koh C, Lovelace CC. Regulation of mitochondrial malic enzyme synthesis in mouse brain. *Proc Natl Acad Sci U S A.* 1979;76(12):6539–6541.
- 44 McKenna MC, Stevenson JH, Huang X, Tildon JT, Zielke CL, Hopkins IB. Mitochondrial malic enzyme activity is much higher in mitochondria from cortical synaptic terminals compared with mitochondria from primary cultures of cortical neurons or cerebellar granule cells. *Neurochem Int.* 2000;36(4–5):451–459.
- 45 Laranjeira A, Schulz J, Dotti CG. Genes Related to Fatty Acid β -Oxidation Play a Role in the Functional Decline of the Drosophila Brain with Age. *PLoS One.* 2016;11(8):e0161143.
- 46 Schulz JG, Laranjeira A, Van Huffel L et al. Glial β -oxidation regulates Drosophila energy metabolism. *Sci Rep.* 2015;5:7805.
- 47 van der Velpen V, Teav T, Gallart-Ayala H et al. Systemic and central nervous system metabolic alterations in Alzheimer's disease. *Alzheimers Res Ther.* 2019;11(1):93.
- 48 Ciavardelli D, Piras F, Consalvo A et al. Medium-chain plasma acylcarnitines, ketone levels, cognition, and gray matter volumes in healthy elderly, mildly cognitively impaired, or Alzheimer's disease subjects. *Neurobiol Aging.* 2016;43:1–12.
- 49 Molsberry S, Bjornevik K, Hughes KC et al. Plasma Metabolomic Markers of Insulin Resistance and Diabetes and Rate of Incident Parkinson's Disease. *J Parkinsons Dis.* 2020;10(3):1011–1021.
- 50 Liu T, Deng K, Xue Y et al. Carnitine and Depression. *Front Nutr.* 2022;9:853058.
- 51 Parksepp M, Haring L, Kilk K et al. A Marked Low-Grade Inflammation and a Significant Deterioration in Metabolic Status in First-Episode Schizophrenia: A Five-Year Follow-Up Study. *Metabolites.* 2022;12(10). doi:10.3390/metabo12100983.
- 52 Kriisa K, Leppik L, Balõtšev R et al. Profiling of Acylcarnitines in First Episode Psychosis before and after Antipsychotic Treatment. *J Proteome Res.* 2017;16(10):3558–3566.
- 53 Lee SGW, Ro YS, Jung E et al. Serum Acylcarnitine and Long-Term Functional Prognosis after Traumatic Brain Injury with Intracranial Injury: A Multi-Center Prospective Study. *J Neurotrauma.* 2023;40(3–4):274–282.

Copyright: © 2023 The authors. This is an Open Access preprint (not peer-reviewed) distributed under the terms of the Creative Commons Attribution License, which permits unrestricted use, distribution, and reproduction in any medium, provided the original authors and source are credited. © remains with the authors, who have granted MitoFit Preprints an Open Access publication license in perpetuity.



Supplement

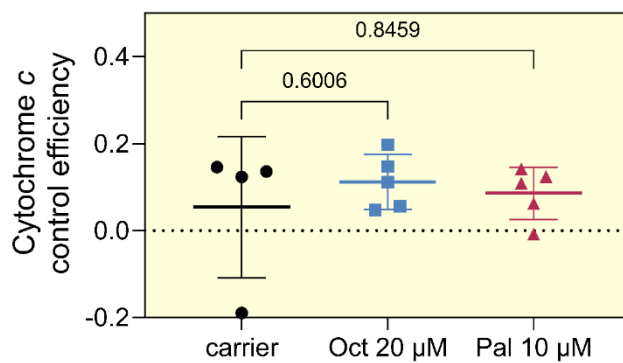


Figure S1. Cytochrome *c* control efficiency in the presence or absence of different acylcarnitines. The presence of acylcarnitines for measurement of FAO did not impact the mitochondrial outer membrane integrity. The cytochrome *c* control efficiency is the flux change after titration of cytochrome *c*. The results are presented as the mean \pm SD of 4–5 independent measurements, and the results were compared with one-way ANOVA.

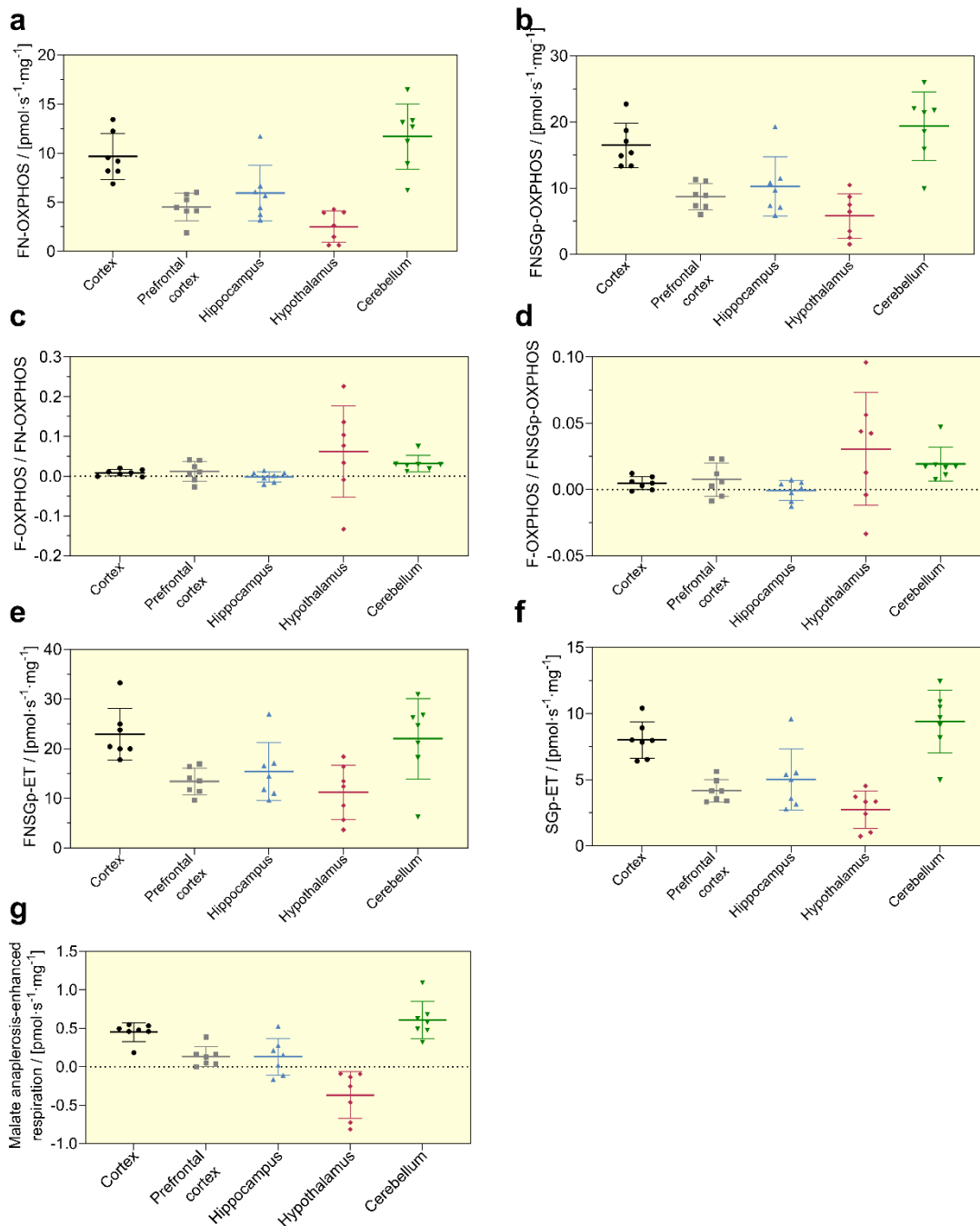


Figure S2. Respiration of mouse brain regions (cortex, prefrontal cortex, hippocampus, hypothalamus, and cerebellum) normalized per tissue protein. The highest overall energy metabolism rate occurred in the cerebellum and cortex, followed by the hippocampus, prefrontal cortex, and hypothalamus: **(a)** FN-OXPPOS capacity in the presence of palmitoylcarnitine, pyruvate, glutamate and, malate. **(b)** FNSGp-OXPPOS capacity with these same substrates plus succinate and glycerophosphate. **(c, d)** Intraexperimental ratios between FAO OXPPOS-capacity and O₂ flux with FN- or FNSGp-pathway substrates, PalPGM or PalPGMSGp, respectively. **(e)** FNSGp-ET capacity, measured after titration of uncoupler; **(f)** SGp-ET capacity, measured following rotenone titration. **(g)** Malate anaplerosis-enhanced respiration, the sum of the stimulation of O₂ flux by 0.1 mM and 2 mM malate titration. Means \pm SD, $N=6$. One-way ANOVA followed by Tukey's test p values are shown in Table S1.

Table S1. *p* values summarized from Figure 6 and S2, Tukey's multiple comparison test following one-way ANOVA.

FAO capacity	Prefrontal cortex	Hippocampus	Hypothalamus	Cerebellum
Cortex	0.9967	0.6065	0.8289	0.0030
Prefrontal cortex	-	0.8079	0.6327	0.0012
Hippocampus		-	0.1189	<0.0001
Hypothalamus			-	0.0416
Malate anaplerosis	Prefrontal cortex	Hippocampus	Hypothalamus	Cerebellum
Cortex	0.0754	0.0721	>0.0001	0.6671
Prefrontal cortex	-	>0.9999	0.0016	0.0028
Hippocampus		-	0.0017	0.0027
Hypothalamus			-	<0.0001
FN-OXPHOS	Prefrontal cortex	Hippocampus	Hypothalamus	Cerebellum
Cortex	0.0034	0.0507	<0.0001	0.5269
Prefrontal cortex	-	0.8102	0.5332	<0.0001
Hippocampus		-	0.0863	0.0009
Hypothalamus			-	<0.0001
FNSGp-OXPHOS	Prefrontal cortex	Hippocampus	Hypothalamus	Cerebellum
Cortex	0.0055	0.0355	0.0001	0.6348
Prefrontal cortex	-	0.9427	0.6229	0.0001
Hippocampus		-	0.2203	0.0010
Hypothalamus			-	<0.0001
FNSGp-ET	Prefrontal cortex	Hippocampus	Hypothalamus	Cerebellum
Cortex	0.0311	0.1279	0.0053	0.9986
Prefrontal cortex	-	0.9655	0.9522	0.0590
Hippocampus		-	0.6565	0.2158
Hypothalamus			-	0.0108
SGp-ET	Prefrontal cortex	Hippocampus	Hypothalamus	Cerebellum
Cortex	0.0027	0.0261	<0.0001	0.5870
Prefrontal cortex	-	0.5870	0.8962	0.5563
Hippocampus		-	0.1380	0.0006
Hypothalamus			-	<0.0001
FAO capacity/FN-OXPHOS	Prefrontal cortex	Hippocampus	Hypothalamus	Cerebellum
Cortex	>0.9999	0.9971	0.3530	0.9239
Prefrontal cortex	-	0.9898	0.4241	0.9582
Hippocampus		-	0.2039	0.7784
Hypothalamus			-	0.8260
FAO capacity/FNSGp-OXPHOS	Prefrontal cortex	Hippocampus	Hypothalamus	Cerebellum
Cortex	0.9992	0.9856	0.1784	0.7014
Prefrontal cortex	-	0.9427	0.2701	0.8309
Hippocampus		-	0.0633	0.3934
Hypothalamus			-	0.8547

Table S2. *p* values summarized from Figure 8, Tukey's multiple comparison test following two-way ANOVA, n.c.: not compared.

F-OXPPOS capacity		Non-risk		Risk		
		ET-1 2 h	ET-1 24 h	Sham 2 h	ET-1 2 h	ET-1 24 h
Non-risk	Sham 2 h	0.9163	0.7349	0.3863	n.c.	n.c.
	ET-1 2 h	-	0.4949	n.c.	0.9797	n.c.
	ET-1 24 h	0.4949	-	n.c.	n.c.	0.0436
Risk	ET-1 2 h	0.9797	n.c.	0.4341	-	0.5603
	ET-1 24 h	n.c.	0.0436	0.0808	0.5603	-

FNS-OXPPOS		Non-risk		Risk		
		ET-1 2 h	ET-1 24 h	Sham 2 h	ET-1 2 h	ET-1 24 h
Non-risk	Sham 2 h	0.7955	0.9156	0.8913	n.c.	n.c.
	ET-1 2 h	-	0.5563	n.c.	0.9166	n.c.
	ET-1 24 h	0.5563	-	n.c.	n.c.	0.0055
Risk	ET-1 2 h	0.9166	n.c.	0.9145	-	0.0963
	ET-1 24 h	n.c.	0.0055	0.0441	0.0963	-

F-OXPPOS capacity/FN-OXPPOS		Non-risk		Risk		
		ET-1 2 h	ET-1 24 h	Sham 2 h	ET-1 2 h	ET-1 24 h
Non-risk	Sham 2 h	0.9835	0.9927	0.5993	n.c.	n.c.
	ET-1 2 h	-	0.9552	n.c.	0.9456	n.c.
	ET-1 24 h	0.9552	-	n.c.	n.c.	0.2307
Risk	ET-1 2 h	0.9456	n.c.	0.8005	-	0.5627
	ET-1 24 h	n.c.	0.2307	0.2596	0.5627	-

F-OXPPOS capacity/FNS-OXPPOS		Non-risk		Risk		
		ET-1 2 h	ET-1 24 h	Sham 2 h	ET-1 2 h	ET-1 24 h
Non-risk	Sham 2 h	0.9305	0.9336	0.4779	n.c.	n.c.
	ET-1 2 h	-	0.7574	n.c.	0.9556	n.c.
	ET-1 24 h	0.7574	-	n.c.	n.c.	0.1270
Risk	ET-1 2 h	0.9556	n.c.	0.5678	-	0.5904
	ET-1 24 h	n.c.	0.1270	0.1556	0.5904	-